REPORT DOCUMENTATION PAGE

Form Approved
OMB No. 0704-0188

PLEASE DO NOT RETURN YOUR FORM TO THE ABOVE ORGANIZATION.

1. REPORT DATE *(DD-MM-YYYY)*	2. REPORT TYPE	3. DATES COVERED *(From - To)*
06-08-2008	Journal Article	

4. TITLE AND SUBTITLE

Patos Lagoon Outflow Within the Rio de la Plata Plume Using an Airborne Salinity Mapper: Observing an Embedded Plume

5a. CONTRACT NUMBER

5b. GRANT NUMBER

5c. PROGRAM ELEMENT NUMBER

0602435N

6. AUTHOR(S)

Derek M. Burrage, Joel C. Wesson, Carlos Martinez, Tabre Perez, Osmar Moller, Jr., A. Piola

5d. PROJECT NUMBER

5e. TASK NUMBER

5f. WORK UNIT NUMBER

73-6629-06-5

7. PERFORMING ORGANIZATION NAME(S) AND ADDRESS(ES)

Naval Research Laboratory
Oceanography Division
Stennis Space Center, MS 39529-5004

8. PERFORMING ORGANIZATION REPORT NUMBER

NRL/JA/7330--06-6220

9. SPONSORING/MONITORING AGENCY NAME(S) AND ADDRESS(ES)

Office of Naval Research
800 N. Quincy St.
Arlington, VA 22217-5660

10. SPONSOR/MONITOR'S ACRONYM(S)

ONR

11. SPONSOR/MONITOR'S REPORT NUMBER(S)

12. DISTRIBUTION/AVAILABILITY STATEMENT

Approved for public release, distribution is unlimited.

13. SUPPLEMENTARY NOTES

14. ABSTRACT

Using brightness temperature *Tb* measurements from L-band airborne microwave radiometers, with independent sea surface temperature (SST) observations, sea surface salinity (SSS) can be remotely determined with errors of about 1 psu in temperate regions. Nonlinearities in the relationship between *Tb*, SSS, and SST produce variations in the sensitivity of salinity *S* to variations in *Tb* and SST. Despite significant efforts devoted to SSS remote sensing retrieval algorithms, little consideration has been given to deriving density *D* from remotely sensed SSS and SST. Density is related to *S* and *T* through the equation of state. It affects the ocean's static stability and its dynamical response to forcings. By chaining together two empirical relationships (flat-sea emissivity and equation of state) to form an inversion algorithm for sea surface density (SSD) in terms of *Tb* and SST, we develop a simple L-band SSD retrieval algorithm. We use this to investigate the sensitivity of SSD retrievals to observed *Tb* and SST and infer errors in *D* for typical sampling configurations of the airborne Salinity, Temperature, And Rough . . .

15. SUBJECT TERMS

sea water, salinity, surface temperature, ocean circulation, river plumes, oceanic fronts, microwave remote sensing

16. SECURITY CLASSIFICATION OF:			17. LIMITATION OF ABSTRACT	18. NUMBER OF PAGES	19a. NAME OF RESPONSIBLE PERSON
a. REPORT	b. ABSTRACT	c. THIS PAGE			Derek M. Burrage
Unclassified	Unclassified	Unclassified	UL	14	19b. TELEPHONE NUMBER *(Include area code)* 228-688-5241

Continental Shelf Research 28 (2008) 1625–1638

Contents lists available at ScienceDirect

Continental Shelf Research

journal homepage: www.elsevier.com/locate/csr

Patos Lagoon outflow within the Río de la Plata plume using an airborne salinity mapper: Observing an embedded plume ☆

Derek Burrage [a,*], Joel Wesson [a], Carlos Martinez [b], Tabare Pérez [c], Osmar Möller Jr. [d], Alberto Piola [e]

[a] Ocean Sciences Branch, Naval Research Laboratory (NRL), Stennis Space Center, MS 39529, USA
[b] Programa de Ciencias del Mar y de la Atmosfera (PCMYA), Seccion Oceanologia, Facultad de Ciencias, Universidad de la Republica, Uruguay
[c] Division de Investigacion y Desarrollo, CITMPSA, Montevideo, Uruguay
[d] Fundação Universidade Federal do Rio Grande(FURG), Campus Carreiros, 96201-900 Rio Grande, RS, Brazil
[e] Departamento Oceanografia, Servicio de Hidrografia Naval, Ciudad Autonoma de Buenos Aires, Buenos Aires, Argentina

ARTICLE INFO

Article history:
Received 20 June 2006
Received in revised form
31 January 2007
Accepted 8 February 2007
Available online 26 March 2008

Keywords:
Sea water
Salinity
Surface temperature
Ocean circulation
River plumes
Oceanic fronts
Microwave remote sensing

ABSTRACT

Major river systems discharging into continental shelf waters frequently form buoyant coastal currents that propagate along the continental shelf in the direction of coastal trapped wave propagation (with the coast on the right/left, in the northern/southern hemisphere). The combined flow of the Uruguay and Paraná Rivers, which discharges freshwater into the Río de la Plata estuary (Lat. ~36°S), often gives rise to a buoyant coastal current (the 'Plata plume') that extends northward along the continental shelf off Uruguay and Southern Brazil. Depending upon the prevailing rainfall, wind and tidal conditions, the Patos/Mirim Lagoon complex (Lat. ~32°S) may also produce a freshwater outflow plume that expands across the inner continental shelf. Under these circumstances the Patos outflow plume can be embedded in temperature, salinity and current fields that are strongly influenced by the larger Plata plume. The purpose of this paper is to present observations of such an embedded plume structure and to determine the dynamical characteristics of the ambient and embedded plumes.

We describe selected results of coincident airborne remote sensing and shipboard in-situ surveys of the salinity distribution and extent of the Plata and Patos/Mirim Lagoon plumes conducted under contrasting winter (2003) and summer (2004) conditions. The surveys were carried out in the context of a comprehensive multi-disciplinary study of the Plata plume and its response to prevailing seasonal weather conditions. The objective was to map the surface salinity distribution of the Plata plume at synoptic scales under representative winter and summer conditions. Additionally, the airborne survey included finer-scale mapping of specific features including the Río de Plata estuarine front and the Patos Lagoon plume, with the objective of determining the distribution and behavior of the plumes in the estuaries and on the continental shelf. The airborne survey was conducted with an aircraft carrying an infrared and microwave radiometer system, the Naval Research Laboratory's (NRL) Salinity, Temperature and Roughness Remote Scanner (STARRS). A series of broad-scale flights over the continental shelf off Argentina, Uruguay and Brazil were made using STARRS to determine the spatial extent of the Plata plume, and detailed mapping flights were undertaken in the vicinity of Río de la Plata Estuary and Patos/Mirim outflows to observe associated frontal features.

The results of the airborne surveys were compared with shipboard hydrographic data obtained from a conductivity, temperature and depth (CTD) profiler. The combined ship and aircraft data were used to estimate parameters of dynamical classification schemes. These schemes were used to characterize the gross behavior and dynamics of the ambient Plata plume and embedded Patos plume. The Plata plume was highly asymmetric with along-shelf development towards the north and it behaved dynamically like a buoyant coastal boundary current, with an approximately geostrophic across-shelf momentum balance. The Patos plume, on the other hand, maintained its integrity as a relatively symmetric, ageostrophic, frictionally dominated plume with significant across-shelf, and modest along-shelf, development.

☆ This paper is dedicated to the memory of Professor Richard W. Garvine University of Delaware, and gratefully acknowledges his many enlightening contributions to the field of coastal ocean dynamics.

* Corresponding author. Tel.: +1 228 688 5241; fax: +1 228 688 5997.
E-mail addresses: burrage@nrlssc.navy.mil (D. Burrage), carmar@glaucus.fcien.edu.uy (C. Martinez), tabare@montepaz.com.uy (T. Pérez), dfsomj@furg.br (O. Möller Jr.), apiola@hidro.gov.ar (A. Piola).

0278-4343/$ - see front matter Published by Elsevier Ltd.
doi:10.1016/j.csr.2007.02.014

The dynamical implications of the embedding of the smaller scale Patos plume within the larger-scale ambient Plata plume were explored, and it was concluded that the ambient plume could exert a significant dynamical influence on the behavior of the embedded plume.

Published by Elsevier Ltd.

1. Introduction

We report here a remote sensing and in-situ observational and dynamical study of the river plume debouching from Lagoa dos Patos (hereafter, Patos Lagoon, and hence Patos Plume) in Southern Brazil, and its embedding within the larger scale plume emanating from the Río de la Plata, which lies between Uruguay and Argentina (Fig. 1). In the context of the circulation of the western South Atlantic, the domain of the Río de la Plata plume (henceforth Plata Plume), which generally propagates northward along the Uruguayan and Southern Brazil coast, spans the west boundary of the confluence region of the poleward flowing Brazil Current (BC) and the equatorward Malvinas Current, and also intersects the associated sub-tropical shelf front, described below.

The literature investigating river plume kinematics and dynamics is extensive, so we give only a brief survey here. Investigations generally fall into three groups. The first uses observations to determine plume distribution and evolution, or to

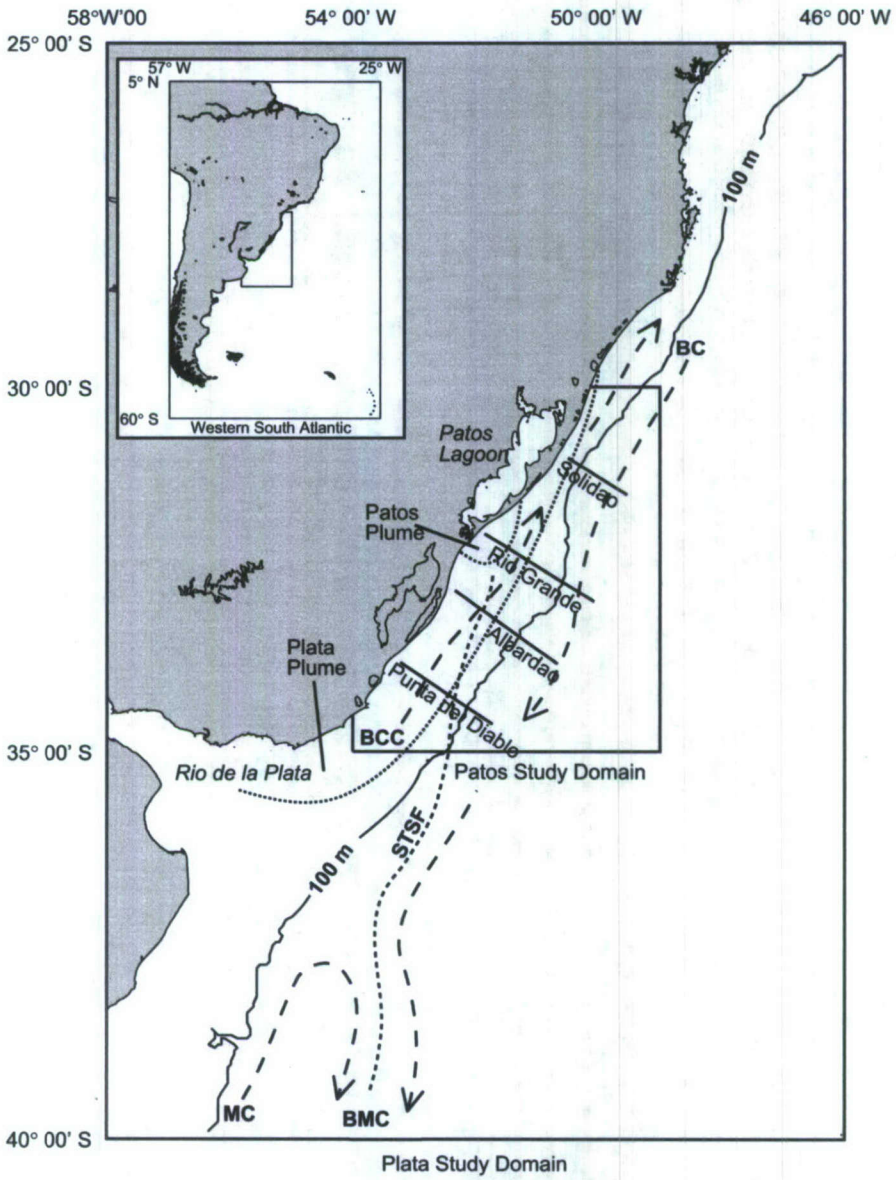

Fig. 1. Map spanning Plata and Patos study domains, with larger scale map of South America and Plata domain inset. The map shows schematically the major ocean currents (dashed lines), the Brazil Current (BC) and Malvinas Current (MC) which merge in the Brazil Malvinas Confluence (BMC), the Brazil Coastal Current (BCC), and representative locations of the Sub-Tropical Shelf Front (STSF, bold dotted line), and the Plata and Patos plumes (light dotted line). The four Plata CTD transects that span the Patos study domains are also indicated (solid lines). (Based on schematics and text presented by Souza and Robinson (2004) and Piola et al. (2005, 2008)).

scale terms in the momentum balance (e.g., Masse and Murthy, 1992; Hickey et al., 1998; Munchow and Garvine, 1993). The second group describes attempts to realistically simulate actual plume behavior numerically under a variety of meteorological and oceanographic forcing conditions (Kourafalou et al., 1996b; Pullen and Allen, 2000; Berdeal et al., 2002). These clearly illustrate instances of plume response to transient forcings, such as shifts between upwelling and downwelling favorable wind. The third group describes analytical or idealized numerical models and classification schemes highlighting the essential momentum balance and plume response (e.g., Chao, 1988; Garvine, 1995, 1999; Kourafalou et al., 1996a; Xing and Davies, 1999; Yankovsky and Chapman, 1997; Yankovsky, 2000; Avicola and Huq, 2002; Fong and Geyer, 2001, 2002; Whitney and Garvine, 2005). The classification schemes span various forcing and boundary conditions including the influence of varying discharge rate, tide and wind stress, and the effects of inlet geometry, shelf bottom slope, bottom friction, and stratification on plume distribution and evolution. However, the effects of along-shelf pressure gradient or ambient boundary currents, and responses to forcing transients (as inferred from observations by Burrage et al. (2002b), and from a numerical study by Fong and Geyer (2002)) have received little attention, and the more complex process of merging of river plumes from disparate sources, which is considered in this paper, has evidently not been addressed.

Synoptic in-situ surveys such as those conducted by Hickey et al. (1998), are difficult to achieve because of the great horizontal extent of large shelf-scale river plumes, and the rapid spatial and temporal changes associated with smaller coastal river plumes. The vertical extent also varies significantly, depending upon river discharge rate, bathymetric slopes and the plumes response to either upwelling or downwelling favorable winds. Satellite or airborne remote sensing can provide more extensive and more frequent views of the surface fields, which can be used to supplement subsurface data, as in studies by Masse and Murthy (1992), Stumpf et al. (1993) and Burrage et al. (2002b c, 2003).

Along the Atlantic continental shelf of South America, a sharp subsurface transition zone, the Subtropical Shelf Front (STSF), exists between the southern source shelf waters, of sub-antarctic origin, and the northern source shelf waters, of subtropical origin (Piola et al., 2000, 2008). The mean location of the STTF trends a little west of south from the mouth of Patos Lagoon (Lat. 32°S) crossing the outer shelf and slope east of Río de la Plata, where it follows the core of the Brazil Malvinas confluence southward into the deep Atlantic (Fig. 1). Possible dynamical links between the STSF, continental runoff and the two western boundary currents have not yet been investigated.

Souza and Robinson (2004) reported results from Lagrangian drifters and AVHRR sea surface temperature (SST) images which show that a northward flowing current, the Brazil Coastal Current (BCC) flows along the continental shelf as far north as Lat. 25°S, in opposition to the BC, which separates from the shelf and flows southward, further offshore. The BC appears over the southern Brazil continental shelf at a location north of Lat. 32°S (Patos Lagoon entrance) during winter and spring and reaches its most northern position, near Lat. 25 S in August. Zavialov et al. (2002) described current measurements made over the shelf during a 5 month period spanning winter, 1997, that indicated only a weak equatorward mean current, masked by wind-driven variability. They also found evidence that stratification associated with high freshwater discharge during winter decouples the subsurface along-shelf currents from surface wind forcing. In any case, the driving mechanism for the BCC is uncertain. It may be related to the large-scale oscillation of the South Atlantic Subtropical Front (STF) and mesoscale eddies spun off from the BC, which it carries northward, in addition to local winds and the discharge of the Río de la Plata and Patos Lagoon.

The hydrological and physical oceanographic properties and processes of the Río de la Plata estuary have been the subject of several observational studies. Framinan and Brown (1996) used NOAA AVHRR visible channel images to study the spatial distribution and seasonal and inter-annual variability in the locations of the turbidity front. Guerrero et al., 1997 analyzed historical river discharge, wind and in-situ temperature and salinity data to determine the horizontal and vertical structure of the front and factors influencing the stratification. Wells and Daborn (1997) provide a comprehensive review of the hydrological, oceanographic and ecological characteristics of the Rio. Simionato and Nunez (2001) modeled the location of the Río de la Plata salinity front using a 3-D baroclinic model to determine factors influencing its seasonal location. River discharge and the wind are the primary factors (Möller et al., 2008). According to Wells and Daborn (1997), the annual mean inflow from the combined Paraná and Uruguay Rivers is 25,000 $m^3 s^{-1}$ (over the period 1983–1992), which is 30% higher than it was during the period 1887–1975. The mean discharge of the Paraná River (1884–1975) is 17,000 $m^3 s^{-1}$ with a maximum of 22,000 and a minimum of 8000 $m^3 s^{-1}$. The mean discharge of the Uruguay River (1916–1975) is 4700 $m^3 s^{-1}$ with a maximum of 14,300 and a minimum of 800 $m^3 s^{-1}$. Since these rivers peak at different times during the year, the seasonal variation of the combined discharge tends to be small (5% of the annual mean).

The results of previous studies in the region (Soares and Möller, 2001; Hubold, 1980a b) show large seasonal variability of the Plata water distribution, with a tendency for equatorward propagation along-shore during the winter, when the prevailing winds are downwelling favorable, and a tendency for offshore spreading during the summer, when the winds are mostly upwelling favorable. Plata water may reach as far north as Lat. 23°S, or nearly 1500 km northward during El Niño winter seasons (Campos et al., 1996). The recognition of the extent of the Plata influence, combined with the fact that no synoptic surveys of the entire plume domain have previously been performed, provided motivation for the development of the international NICOP/PLATA project, of which this study is a part.

The hydrology and oceanography of the Patos Lagoon plume, has also been closely investigated. This Lagoon is 250 km long, 40 km wide and approximately 5 m deep and is connected to the South Atlantic Ocean by a natural channel (modified by training walls) that is about 1 km wide and 12 m deep (Möller et al., 2001). The Lagoon drains a 200,000 km^2 hydrological basin formed primarily by the Guaiba and Camaquã Rivers, which exhibit high discharge in late winter and early spring and low to moderate discharge in summer and autumn. The mean annual discharge is 2000 $m^3 s^{-1}$ (Vaz et al., 2006) but peaks of 12,000–25,000 $m^3 s^{-1}$ have been observed. Seasonal means range from 700 $m^3 s^{-1}$ in summer to 3000 $m^3 s^{-1}$ in spring (Möller et al., 2001). Fernandes et al. (2002) citing unpublished work by Möller, reported that peak discharges of 8000 and 12,000 $m^3 s^{-1}$ have been observed during El Nino events. They reproduced a Radarsat image recorded in April, 1998 showing the plume with a bulge extending 20 km offshore covering an area of 1500 km^2, while Zavialov and Möller (2000), found the plume propagation may extend 50 km from the estuary mouth.

Möller et al. (1996) studied the summertime circulation and dynamics of the Lagoon by analyzing time series of freshwater discharge, wind stress and water level and results from a quasi-steady-state barotropic numerical hydrodynamic model. They found that the longitudinal wind stress generated a set-up and set-down oscillatory response separated by a mid-Lagoon nodal line with a period set by the passage of atmospheric fronts.

The longitudinal momentum balance was dominated by setup equilibrium (wind stress opposing pressure gradient) in the deeper water and by friction in the shallower water, while the lateral momentum balance tended to be geostrophic in both these regions. The wind-forced circulation displayed separate cells in the sub-basins, with downwind current near the margins and upwind return flows in the central areas. The tidal signal was only important near the coastal entrance.

Möller et al. (2001) studied the influence of local versus non-local forcing effects on the Lagoon subtidal circulation. Using spectral analysis of river discharge, sea level and wind observations they found that the local wind was responsible for most of the observed water level variance in the central and inner parts of the Lagoon, while the non-local winds tended to drive the exchanges between the estuarine area and the adjacent continental shelf. Freshwater discharge, however, dominated the dynamics of the entire Lagoon during high flood periods.

Zavialov et al. (2003) reported results of a hydrographic cruise that mapped salinity and temperature features connected with freshwater discharges of the Plata River and Patos Lagoon. They observed a belt of low salinity water, 10 psu fresher than ambient shelf waters extending hundreds of kilometers northward from the Plata River. They also observed strong temperature inversions in the upper layer caused by a combination of advection and surface cooling during winter (Möller et al., 2008, found similar features). A fine-scale survey conducted in late autumn, 2002 revealed a modest Patos Lagoon plume extending at least 10 km offshore but with an area of only 700 km^2. This plume was characterized by salinities of 27 psu near the coast with a sharp salinity front of 2–3 psu contrast near the Lagoon entrance. Despite the training walls that direct the outflow initially toward the south (poleward), the plume penetrated less than 5 km in this direction. Instead, it was immediately detached from the coast and veered offshore and toward the east.

Fernandes et al. (2004) studied the attenuation of tidal and subtidal oscillations in the Patos Lagoon estuary. Using spectral analysis, they found that both high-frequency (tidal) and low-frequency (sub-tidal) oscillations decreased progressively inside the Lagoon, but were less attenuated during summer than during winter, when freshwater inflows and wind effects tended to dominate. The sub-tidal oscillations were also less attenuated than the tidal oscillations. The entrance channel thus acts as a filter for tidal, and to a lesser extent, sub-tidal signals.

Much is known about the hydrological and hydrographic characteristics of the Plata river basin, estuary and ocean outflow plume, including its response to river discharge and wind stress variations. The hydrological characteristics of Patos Lagoon are also relatively well known, but there are important gaps. For example, the inflow from the Mirim Lagoon complex can be a significant source of freshwater and sediment, but it is not gauged. The remaining mean discharge is a small fraction (about 1/10th) of that of the Plata, and is subject to greater seasonal and interannual variability. The hydrodynamics of the Lagoon, including its response to discharge, wind and tide has been well studied, and there is some knowledge of the estuarine zone, including water mass exchange with the continental shelf. A limited number of observational studies provide a basic description of the circulation on the continental shelf. However, the separate impact of the two plumes on the shelf circulation and the interaction between the Plata and Patos outflow plumes have not been studied. This paper seeks at least a partial remedy to this deficiency, by investigating the kinematics and dynamics of the two plumes and their interaction, using airborne and in-situ observations.

Section 2 describes the observational methods and classification schemes used in the study. Section 3 describes the plume kinematics. Section 4 classifies the plumes dynamically based on observable parameters. Section 5 discusses the dynamical implications of plume embedding and Section 6 summarizes the conclusions.

2. Methods

The Río de la Plata and Patos Lagoon plumes were surveyed in winter and summer 2003–4 using a combination of airborne remote sensing and shipboard in-situ measurements of surface and sub-surface temperature and salinity. The two methods are mutually complementary. The in-situ conductivity, temperature and depth (CTD) measurements are more accurate and more precise than the airborne microwave radiometer measurements, and they provide sub-surface profiles at specific locations. They allow a 2D vertical section of near and sub-surface temperature, salinity and density to be constructed from data acquired over a period of one to several days. In contrast, the remotely sensed data have the advantage of rapid spatial coverage of surface fields. They allow horizontal transects, or 2D maps, of temperature, salinity and density to be constructed on nearly synoptic scales, over a period of several hours. The combined hydrographic data from the aircraft and ship platforms were used to characterize the river plume and to determine parameters describing plume size and shape, that could not be obtained from surveys conducted exclusively using ships.

2.1. Airborne salinity mapping

Airborne mapping of sea surface salinity was carried out using the Naval Research Laboratory (NRL) Salinity, Temperature and Roughness Remote Scanner (STARRS), mounted on a Uruguayan Air Force Casa 212 Aviocar twin-engined aircraft. STARRS is a system comprising L and C-band microwave radiometers for remotely sensing surface salinity and roughness, respectively, and an infra-red radiometer to determine SST. The technology, performance, and installation and deployment of STARRS during the Plata project are described, respectively, in Burrage et al. (2002a) and Miller and Goodberlet (2004), Burrage et al. (2006) and Pérez et al. (2006). A laboratory calibration of STARRS was carried out prior to and following each of the two surveys using methods similar to those described by Prytz et al., 2002 for an earlier generation of instrument, the Scanning Low Frequency Microwave Radiometer, SLFMR. The resulting brightness temperature accuracy is considered to be approximately ± 1.0 K, which corresponds to a salinity accuracy of about ± 2 psu.

The research involved two missions that were synchronized with oceanographic cruises conducted in August 2003 during the austral winter (Piola et al., 2003, Martinez, 2003; Pérez et al., 2006), and in February 2004 during the austral summer (Möller and Piola, 2004). Both extensive line-transect surveys and intensive mapping surveys were conducted. The extensive surveys (Martinez, 2003) closely followed the ship tracks (Piola et al., 2003). Each mission lasted approximately 10 days, and reasonable synchronicity with the ship operations was achieved. In this paper, we focus mainly on the results of the wintertime survey, during which the Plata and Patos plumes were well developed.

2.2. Ship hydrosurveys

Shipboard hydrosurveys were conducted using a Sea Bird Electronics 911 Plus CTD calibrated by the manufacturer, along with various other oceanographic instruments (Piola et al., data report & URL). The first cruise, of the Argentine Navy

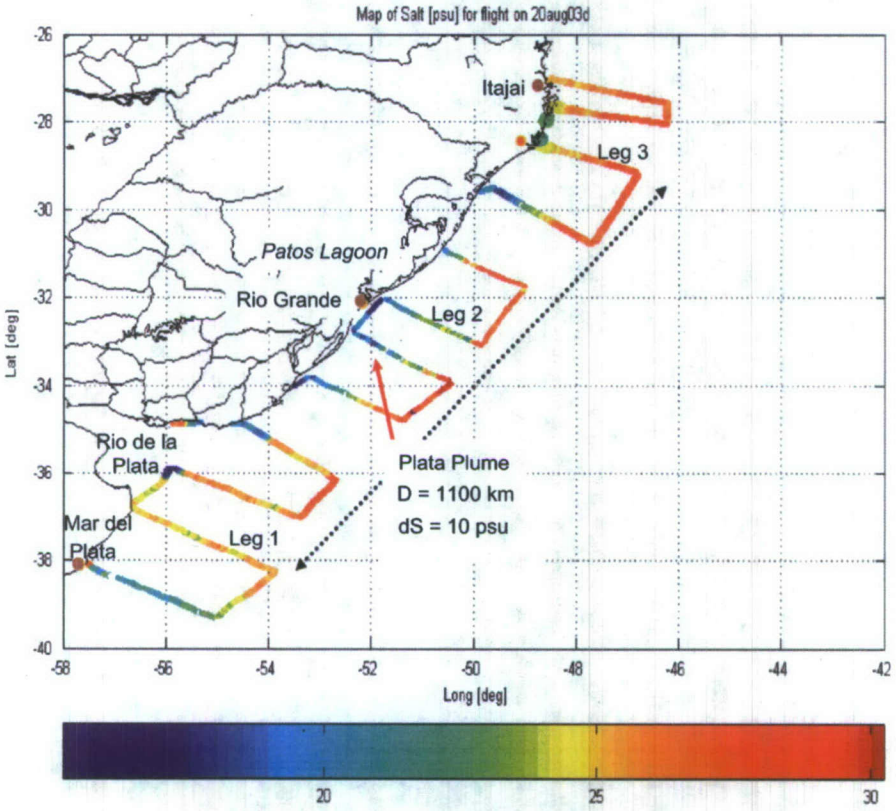

Fig. 2. Plata plume extensive airborne salinity survey conducted using STARRS in winter 2003. The plume, indicated by low salinity water north of Lat. 37.5°S extends approximately 1100 km along the coast from the Río de la Plata estuary separating Uruguay and Argentina to Itajai in southern Brazil. The across-shelf salinity contrast is approximately 10 psu. A lower salinity patch of water off Rio Grande indicates the embedded Patos plume (See Fig. 3).

oceanographic research vessel *Puerto Deseado*, was conducted from 20 August 2003 to 2 September 2003. The second, on the Brazilian Navy research vessel *Antares*, was conducted from 1 to 19 February 2004. Meteorological observations were also recorded manually from the bridge and from the ship's meteorological instruments. Key results of these hydrosurveys are presented by Piola et al., 2008 and Möller et al., 2008. Only those results that are pertinent to the Plata and Patos plume sea surface salinity remote-sensing surveys are presented in this paper.

2.3. Plume data acquisition

Nearly synoptic airborne scale surveys (or flight legs, Fig. 2) were conducted over three different sections of the Plata plume during the evenings of 20 August (Leg 1), 31 August (Leg 2) and 2 September, 2003 (Leg 3). Each leg, which comprised 4 across-shelf transects and 3 along-shelf transects was completed during a 7–8 h flight. Together the three legs spanned the period of the wintertime cruise of the *Puerto Deseado*. A similar survey was conducted during the summer using the Casa 212 and *Antares*. However, the Patos outflow plume was not extant d uring that survey. The salinity values shown were computed using a preliminary calibration of the STARRS L-band brightness temperature data, following the method described by Burrage et al., 2002c, and should not be regarded as accurate in the absolute sense. Comparison with the shipboard near-surface CTD data, which are derived from typical depths of 3–4 m (Piola et al., 2003), shows that STARRS surface salinities acquired during the extensive survey were fresher by about 6 psu, which could suggest the existence of a STARRS calibration bias. This could also be a reflection of near-surface stratification, since the depth of penetration of the STARRS L-band measurement is only a few centimeters, while the CTD data are acquired, as noted, from depths of several meters. In spite of the apparent inaccuracy, we believe the STARRS data are sufficiently precise to give a good indication of relative salinity values (Burrage et al., 2006). Thus, the salinity difference across the plume boundary should be well represented.

The Patos Plume was mapped using STARRS during the intensive survey on the evening of 1 September 2003 (Fig. 3), which was conducted in the region surrounding the entrance to Patos Lagoon. In the intensive survey, the salinity bias was removed by adjusting the salinity offset to approximately match the salinity measurements available from the ship observations.

2.4. Plume classification schemes

As a starting point in the analysis of the embedding of the Patos plume within the Plata plume, and to provide a basis for a numerical modeling study of the plume embedding and merger process (Burrage et al, in preparation), it is useful to determine the gross features of the observed plumes, and use these to determine their major dynamical characteristics. A generalized description of plume dynamics might allow certain simplifications to be made in assessing the influence of the larger ambient plume on the smaller embedded plume, and should provide useful guidance in interpreting numerical model results.

The plume dynamics may be systematically described using various diagnostic schemes. These have been developed for particular combinations (subsets) of the full set of terms in the

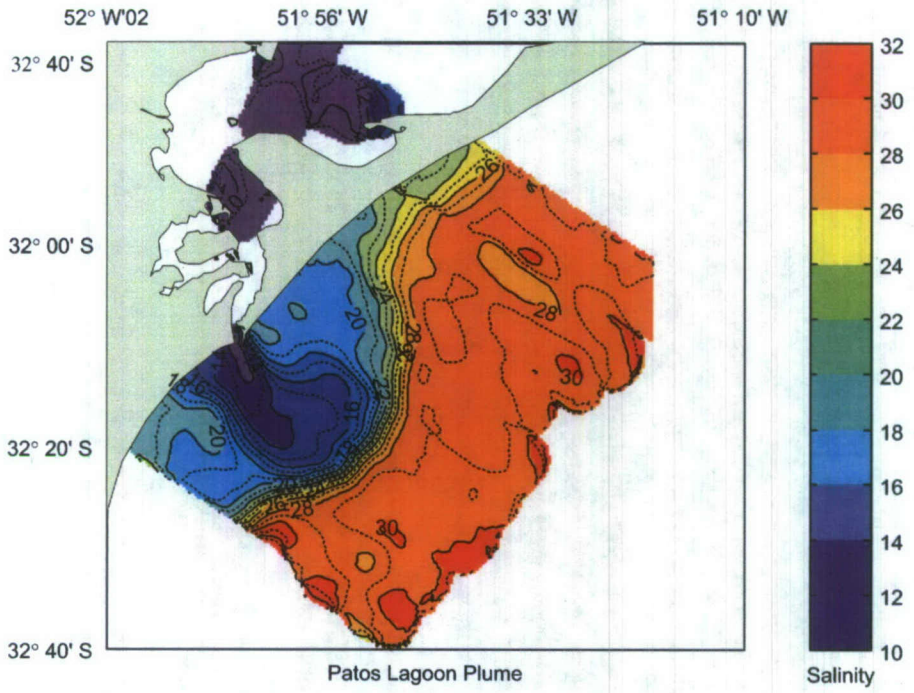

Fig. 3. Patos plume intensive airborne salinity survey conducted using STARRS in winter 2003. Plume salinity ranges from 12 to 27 psu, with salinity contrast in the frontal region of approximately 10 psu. It is 33 km wide with a length exceeding 100 km. Its shape suggests a weakly asymmetric excursive bulge with anti-cyclonic veering, and a weak, low aspect ratio equatorward coastal current.

momentum balance of the plume and its ambient receiving waters. While not all these were intentionally developed as classification schemes, it is convenient to refer to them as such, because of their utility for that purpose. Among the small number of available schemes, we chose those which could best utilize our survey data. Each of the selected classification schemes, which we denote G95—Garvine (1995), G99—Garvine (1999), A&H—Avicola and Huq (2002), W&G—Whitney and Garvine (2005) and C88—Chao (1988) focuses on a particular class of forcings. They also depend upon specific assumptions and observables (dimensional parameters) needed to derive non-dimensional parameters useful for comparing and classifying particular plumes. All of them assume a steady state, so the effects of the local acceleration term in the momentum balance, and of transients in the various forcing fields, notably of wind and sea level, are not explicitly taken into account. To address this deficiency, we can determine the relative importance of these forcing terms in the steady state, then assess the time scales of variation of the dominant terms to determine, a posteriori, if they are likely to be significant. Most also assume a Margules frontal structure (in thermal wind balance) in constructing certain non-dimensional scales. This implies that the flow is essentially two-layered, rather than continuously stratified, and that the seabed is essentially horizontal, rather than sloping.

The classification scheme of Garvine (1995), G95, ranks plumes primarily on the basis of Kelvin number, K, which is the ratio of plume width to the baroclinic Rossby radius. For plumes with small K values, momentum advection terms tend to dominate Coriolis effects. Such plumes are little affected by earth rotation and are usually, but not always, of smaller geographic scale. In contrast, those with high K values tend to be geostrophically balanced. These are usually of larger geographic scale. The scheme employs a number of secondary parameters, including the Froude number, F, which tends to vary inversely to K, being higher/lower for smaller/larger-scale plumes, respectively. Other secondary parameters describe plume aspect ratio (elongation) and tendencies to response to stresses imposed at the surface (wind) and bottom (bed friction).

The scheme of Garvine (1999), or G99, focuses on along-shelf penetration of the plume under the influence of river discharge, but ignores the influence of the wind. Analytically, the along- and across-shelf penetration are determined by five non-dimensional parameters that describe the source transport, inlet width, bottom slope, tidal current intensity and the inlet aspect ratio. However, the scheme comprises an analysis of numerical model behavior and this introduces two additional, empirical and somewhat arbitrary, terms due to vertical and horizontal eddy diffusivity.

The classification scheme of Avicola and Huq (2002), A&H, reveals the extent to which a plume may be considered bottom-trapped (deep) or surface-advected (shallow) according to whether the non-dimensional ambient depth parameter, h/H, is high or low, respectively (here, h is plume scale depth and H is ambient ocean depth). It also reveals the extent to which its width at the base, where it intersects the bed, is compressed or expanded horizontally across-shelf, relative to its scale width, the internal Rossby radius, R. This is determined according to whether its (non-dimensional) bottom slope parameter, R/y_b (where y_b is the offshore extent of the bottom-trapped layer), respectively, high or low. According to the scheme, a plume with a high/low slope parameter value, being compressed/expanded at its base, has a stronger/weaker internal pressure gradient, and thus steeper/shallower isopycnal slopes and stronger/weaker geostrophic currents.

The combined effect of winds and river discharge is represented in the scheme of Whitney and Garvine (2005), W&G, in which a wind strength index, W_S, determines whether the plume flow is primarily wind or buoyancy driven, while a tilt time scale, t_{tilt}, determines how quickly the plume circulation responds to the wind-driven Eckman forcing. The relative size of these two parameters determines the tendency of the plume to narrow or

expand in width, in response to downwelling and upwelling favorable winds.

Chao (1988), C88, used his scheme to study the development, maintenance and dissipation of river plumes both with and without a seaward sloping bottom. He classified plumes on the basis of an empirical Froude number, V_m/C_O, and a dimensionless phase speed C/C_O, that determines the influence of dissipation. Here, V_m is the inflow speed at the estuary mouth, C_O is inviscid internal gravity wave phase speed, and C is instantaneous intrusion speed downstream of the mouth. Four plume classes were identified: supercritical, subcritical, diffusive-supercritical and diffusive-subcritical. A supercritical plume has an excursive bulge near the inlet and a relatively narrow coastal jet downstream; the excursion tends to be enhanced by seaward bottom slope. For subcritical plumes, the bulge is reduced to a width comparable with that of the coastal jet. For diffusive plumes, mixing tends to retard the plumes intrusion and limit the bulge's seaward excursion, regardless of its criticality.

3. Plume kinematics

Here we describe results obtained from the ship and aircraft measurements that can be used to infer the plume's geometric and internal properties on near-synoptic time and space scales. The results are used in Section 4 to determine non-dimensional parameters for the various plume classification schemes, and the magnitudes of terms in the steady-state momentum balance of the plume.

3.1. Plata plume

The aircraft survey of the Plata plume (Fig. 2) shows a band of low salinity water flowing equatorward along the coast from the northern side of the Río de la Plata estuary (Lat. 35°S) to Itajai (28°S), a distance of about 1200 km. This feature was similarly observed by the ship. A relatively sharp salinity front marked, for this preliminary calibration, by the 24 psu isohaline can be traced along the inner shelf. This originates from inside the estuary and its shape shows that the plume thickness varies along the coast, being widest just south of Rio Grande (in Leg 2), near the entrance to Patos Lagoon, and narrower elsewhere, except near Itajai, where it terminates near the coast. In the shipboard data this frontal line closely follows the 32 psu isohaline. If, instead, the 27 psu STARRS isohaline is taken to define the plume boundary, the width appears to change in the same manner but it naturally appears wider. In the shipboard data this line closely follows a 2 psu front separating isohalines of 34 and 36 psu. In this case it is not clear whether some of the fresher water surrounding the entrance to the estuary originates in the Río de la Plata, or is derived from further south. The most saline water detected by STARRS and the ship was, respectively, 30 and 36 psu. This lies near the shelfbreak where the freshwater influence is likely minimal, surface mixing is likely enhanced, and the near surface stratification should be weak. Here STARRS exhibits the −6 psu bias mentioned earlier, and the additional −2 psu difference in the frontal zone is likely accounted for by surface freshening. As a general rule, Piola et al. (2008) define the Plata frontal boundary to coincide with the 33 psu isohaline, which in our shipboard survey lies about 130 km (70 N m) offshore at Rio Grande (Fig. 4). Allowing for the bias, this would coincide with the 27 psu STARRS isohaline, described above, which extends further seaward than the ship 33 psu line. Due possibly to surface freshening, the front detected by STARRS, virtually at the surface, thus indicates a wider plume than that indicated by the ship's (subsurface) 33 psu isohaline. In any case, based on these findings the surface front of the Plata plume appears to have an average width of about 185 km (100 N m), giving the plume an aspect ratio, of width to length, of approximately 1:11.

3.2. Patos plume

The Patos plume may be identified in the extensive survey (Fig. 2) by a small patch of extremely low salinity (~15 psu) water situated immediately offshore from Rio Grande (Lat. 32°S, Long. 52°W). Although the absolute accuracy of this survey should be regarded as uncertain, it is clear from the inner shelf location of the survey that the Patos plume is fully embedded within the Plata plume, as observed in the intensive aircraft and ship surveys. Since the minimum near-surface salinity observed in the Plata plume from the ship (at the inshore end of transects located south of the Patos Lagoon entrance) was about 27 psu (Piola et al., 2003), this could be adopted as an indicator for the maximum salinity associated with the Patos plume. Based on this definition, the plume has a maximum width of about 33 km (18 N m) and salinity contrast of 12 psu (range 15–27). Since the south-western plume boundary was not mapped, it is not possible to accurately determine its length. However, if we assume the plume is approximately symmetrical, as suggested by the locus of the 19 psu isohaline, the length of the eastern half suggests a total length of about 100 km (55 N m). This gives an aspect ratio of about 1:3, which is smaller than that of the Plata plume by a factor of nearly 4.

The Patos Plume was not observed in any detail by the shipboard survey, but its presence is indicated in the vertical salinity section obtained along the Rio Grande transect (see Fig. 4c), which coincides closely with that obtained from the STARRS across-shelf transect (Leg 2) in Fig. 2. An additional contribution of freshwater, possibly derived from the Patos plume, is evident in the downstream direction at the more northerly Solidão ship transect, which shows a freshening near shore relative to the upstream Albardão transect. The latter is likely influenced exclusively by the Plata plume.

3.3. Shelf hydrography

In these wintertime vertical sections, the salinity (Fig. 4a, c, e) and temperature (Fig. 4b, d, f) in the deeper water compensate in their effect on density and the salinity strongly dominates the density field (Fig. 5a, c, e). Offshore in water deeper than about 40 m, the structure of the temperature appears similar to that of the salinity field (the fields are correlated). In these waters there is a large retrograde frontal structure, the STSF (Piola et al., 2008; Möller et al., 2008) which, if associated with the Plata plume, would indicate that the latter is both continuously stratified (rather than sharply layered), and attached to the bottom. In waters shallower than 40 m, which lie on the inner continental shelf, the temperature field appears vertically well mixed. This tendency for homogeneity in the temperature field from Punta del Diablo, north to Rio Grande is a characteristic of the Plata plume water in winter (Möller et al., 2008). In contrast, the salinity field shows a retrograde frontal structure in both the Solidão (Fig. 4a) and Albardão (Fig. 4e) sections, but in the Rio Grande section (Fig. 4c), which is dominated by the presence of the Patos plume, and in waters shallower than 20 m, it appears vertically homogeneous. The strong horizontal density gradient (Fig. 5c) that appears near the coast off Rio Grande (barely resolved spatially at the left side of the plot) is dominated by the low salinity Patos Lagoon plume (rather than temperature, which varies over larger scales).

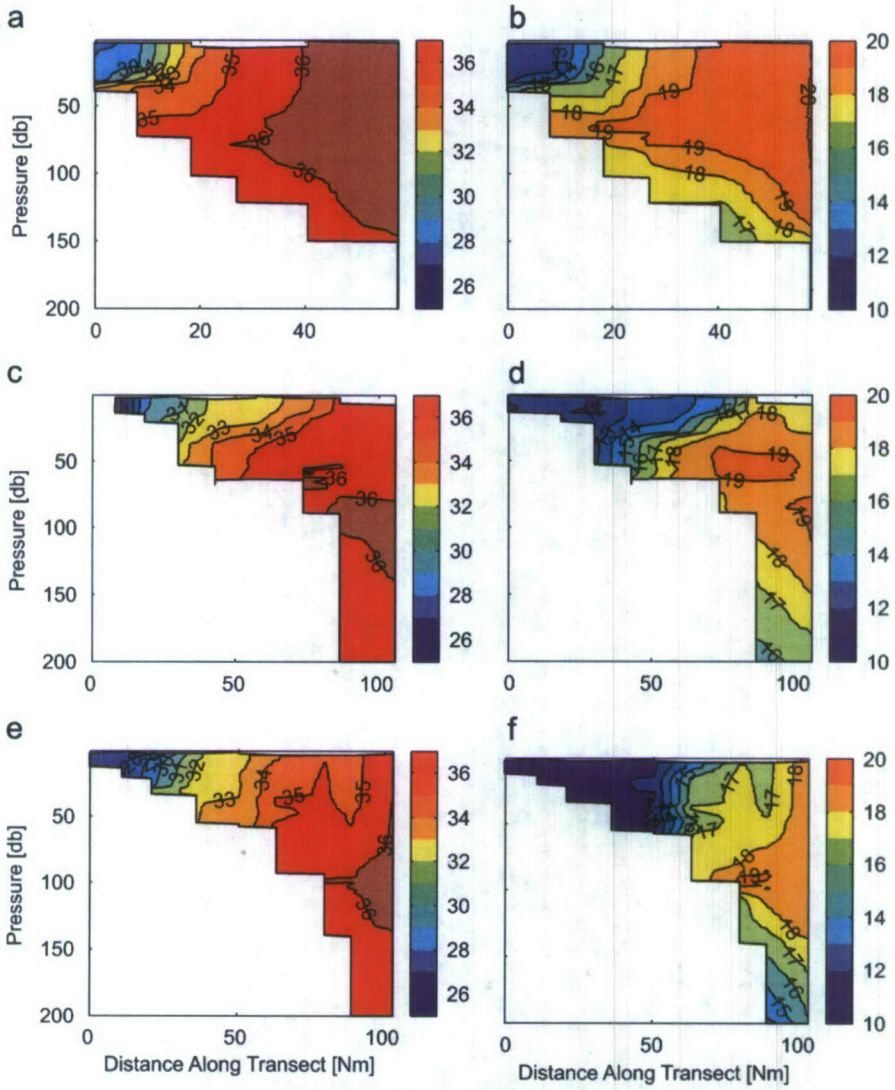

Fig. 4. Vertical sections of temperature (T90) and salinity for the winter, 2003 Solidão, Rio Grande, and Albardão CTD sections. Low-salinity coastal water (13–35 psu) influenced by the Plata plume is evident in all 3 sections, and a patch of vertically well-mixed water of lower salinity (< 13 psu) due to the Patos plume is evident off Rio Grande: (a) Solidao salinity (psu), (b) Solidao T90 (deg C), (c) RioGrande salinity (psu) (d) RioGrande T90 (deg C), (e) Albardao salinity (psu), (f) Albardao T90 (deg C).

While the horizontal resolution is limited by the relatively large CTD station spacing, this vertical homogeneity suggests that the Patos plume is not only bottom attached, but unstratified close to the Patos Lagoon entrance. Mixing associated with strong tidal currents ($\sim 2\,m\,s^{-1}$) through the narrow Lagoon entrance might account for this effect (Fernandes et al., 2004). Strong seaward flow has been observed during NE wind events associated with high river discharge (Möller and Castaing, 1999). However, wind does not appear to be a significant factor in the nearshore mixing at the time of our observations. Winds were only $5–10\,m\,s^{-1}$ near the shore during the conduct of the Albardão, Rio Grande and Solidão survey transects. However, they were $10–20\,m\,s^{-1}$ offshore (Fig. 6) and stronger at the time the Solidão transect was conducted. This might account for the relatively deep mixed layer evident over the outer shelf in that transect. In contrast, the relatively shallow Punta del Diablo transect (not shown, located south of the Albardão transect, see Fig. 1) was conducted during strong winds $15–25\,m\,s^{-1}$, and it appears vertically well-mixed across the shelf.

Geostrophic velocities computed from the density field, using the surface as reference, indicate southward flow relative to the surface, both at depth and offshore (Fig. 5b, d, f). With mean surface drift equatorward in winter (Zavialov et al., 2002; Souza and Robinson, 2004), the negative relative velocities indicate vertical and horizontal shear with either weaker (equatorward) or reversed (poleward) flows at depth, and seaward. Southward tending current cores appearing in these sections might be due to the BC, or associated mesoscale eddies which tend to encroach on the shelf in the northern part of the domain as observed by Piola et al. (2008). Whether the geostrophic shear that appears on the inner shelf in all three sections ($0.35\,m\,s^{-1}$ off Solidão and $0.25\,m\,s^{-1}$ off Albardão and Rio Grande) is associated with these boundary current features, the Plata plume, or both, they are expected to add significant, mainly cyclonic, vorticity to the Patos plume.

4. Dynamical classification

Dimensional parameters for the Patos and Plata plumes are presented in Table 1, in which their relevance to particular classification schemes is marked by an "X". These parameters

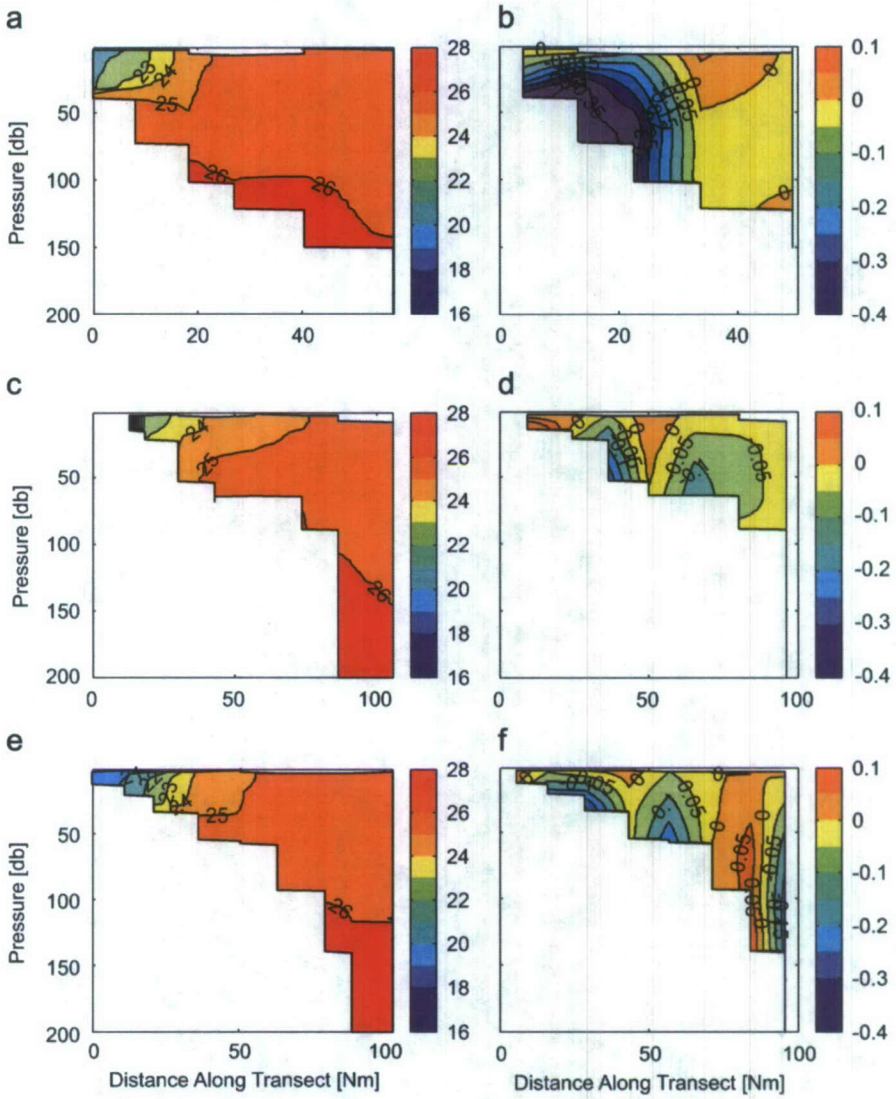

Fig. 5. Vertical sections of Sigma-*t* and geostrophic velocity (relative to the surface) corresponding to the temperature and salinity sections of Fig. 4: (a) Solidao Sig_Theta (kg/m^3), (b) Solidao Gvel (m/s), (c) RioGrande Sig_Theta (kg/m^3), (d) RioGrande Gvel (m/s), (e) Albardao Sig_Theta (kg/m^3), (f) Albardao Gvel (m/s).

were determined using a combination of the aircraft and ship temperature and salinity surveys (for determining plume geographic scales and sea water densities), shipboard wind data, assumptions made by the scheme authors (e.g., the bottom friction coefficient from Garvine, 1995), or values obtained from the literature (along-shelf velocity scale from Soares and Möller, 2001). Classification based on the non-dimensional parameters of the Garvine (1995) (G95) scheme (Table 2, Fig. 7) places the Patos and Plata plume near the lower and upper levels of the bulk Kelvin number, *K*, range, for the cases that he considered (see Garvine, 1995 and his Table 1). For the Plata plume, we found *K* and *F* values of 5.3 and 0.04, respectively, which are comparable with values of 7.7 and 0.02 found by Soares (2003). For the Patos plume our Froude number, *F* was ~0.1. Soares (2003) found a larger *F*~1, but with a discharge larger by a factor of 2 than the annual average value of 2000 m^3 s^{-1} we used, his estimated plume current velocities were probably higher. A few of Garvine's entries for other plumes are reproduced here, for comparison. Results obtained using remote sensing and in-situ measurements of two Australian river plumes by Burrage et al. (2002b) are also shown. The Burdekin River plume was observed to embed the smaller Herbert River plume. The dynamics of the Burdekin and Herbert are comparable with those of the Plata and Patos, respectively. However, the Patos is more strongly affected by basal friction than the Plata, while the Herbert and Burdekin, in this respect, are similar; and the Burdekin is more highly influenced by Coriolis rotation.

The Patos plume has a Kelvin number, *K*, that is intermediate between those of the Gaspe and Algerian currents. However, the secondary parameters, including Froude number *F*, the product *KF*, and the inverse aspect ratio, G^{-1} are all smaller, implying a relatively short sub-critical plume that is less influenced by rotation, while the wind, V_E/HU (Ekman transport) and bottom stress, r/fH terms are larger, implying greater frictional influence (Fig. 7). The resulting momentum balance (Table 3) reinforces this interpretation. In the along-shelf momentum balance, the internal pressure gradients of the plume (assumed in G95 to be of order one) are balanced by a combination of wind, bottom friction and Coriolis force in decreasing order of importance. The across-shelf balance is similar, but the stress terms are of lesser importance, due to the dynamical influence of the aspect ratio on currents.

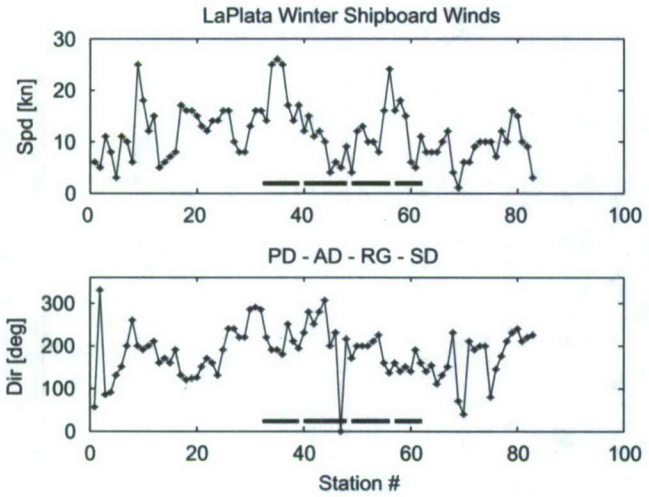

Fig. 6. Shipboard wind measurements, as a function of station number, show that during the CTD survey winds blew predominantly from the SW (range S–W quadrant) with typical speeds of 15 knots (range 5–25 knots). The stations occupied during the Punta del Diablo (PD), Albardão (AD), Rio Grande (RG) and Solidão (SD) transects are indicated.

Table 1
Classification scheme dimensional scale parameters employed in our application to the Plata and Patos plumes (see text for scheme references)

Scale parameter (unit)	Patos winter	Plata winter	G95	G99	A&H	W&G
Latitude (°)	−32	−32	X	X	X	X
Along-shelf flow ($m\,s^{-1}$)	0.1	0.1	X			X
Along-shelf length (km)	100	1100	X		X	
Across-shelf length (km)	33	185	X			X
Plume depth (m)	10	70	X			
Ambient density (Sigma-*t*)	1023	1026	X	X	X	X
Inlet density (Sigma-*t*)	1011	1015	X	X	X	X
Along-shelf wind stress (Pa)	0.081	0.044	X			X
Friction coeff. ($m\,s^{-1}$)	0.001	0.001	X			
Inlet breadth (km)	0.75	220		X		
Discharge ($m^3\,s^{-1}$)	2000	30,000			X	X
Shelf slope	0.0011	0.0011			X	
Inlet depth (m)	12	15			X	
River density (Sigma-*t*)	1000	999				X

Table 2
Derived non-dimensional parameters for G95 Classification scheme

Plume	*K*	*F*	*KF*	1/*G*	V_E/HU	r/fH
Gaspe	2	0.4	0.8	10	0.01	0.1
Patos	**2.4**	**0.09**	**0.22**	**3**	**0.63**	**0.65**
Rhine	3	0.1	0.3	5	0.2	0.7
Algerian	3	0.3	0.9	8	0.01	0.06
Delaware	4	0.1	0.4	5	0.3	0.4
Norwegian	4	0.1	0.4	10	0.01	0.02
Plata	**5.3**	**0.04**	**0.19**	**5.9**	**0.09**	**0.09**
Scottish	10	0.1	1	5	0.05	0.1

Selected results from Garvine (1995) Table 1 that span the *K* values of the Patos and Plata plumes are included for comparison.

The Plata plume *K* value falls between those of the Norwegian and Scottish coastal currents, showing that the Plata is dynamically larger in scale than the Patos. As pointed out by Garvine (1995), this is not necessarily indicative of large physical scale (the Mississippi plume, which is physically large, has a low Kelvin number), but rather emphasizes the importance of rotation, consistent with semi-geostrophic dynamics. The secondary parameters of the Plata (plotted against the primary parameter, Fig. 7) show similar tendencies to those of the Patos plume, with smaller rotation terms (*K*, *KF*) and larger stress terms (V_E/HU, r/fH) than its companions in the table, but the inverse aspect ratio is intermediate, so in contrast to the Patos plume, its elongation is consistent with its companions rather than reduced. The momentum balance is consistent with this interpretation, tending toward geostrophy in both the along- and across-shelf directions, but with significantly more frictional influence in the along-shelf momentum balance. The Plata appears therefore to be essentially semi-geostrophic like its companions. However, with some momentum unaccounted for, it might not be entirely geostrophic even in the across-shelf direction (the order 1 pressure term appears to dominate the sum of all other terms).

Non-dimensional parameters for the classification scheme of Avicola and Huq (2002) are given in Table 4. These are derived from the corresponding dimensional parameters (cols 3–6). The Ambient Depth Parameter h/H (col 1) indicates the degree to which the plume is bottom trapped (deep) or surface advected (shallow). The Bottom Slope parameter, R/y_b (col 2), indicates the extent to which its width at the base, where it intersects the bed, is compressed or expanded across the shelf. In a plot of h/H versus R/y_b (Fig. 8), plumes with high or low h/H values (vertical axis) tend to be bottom-trapped or surface-advected, respectively, while, plumes with high or low R/y_b (horizontal axis) tend to have steeper or shallow isopycnal slopes, respectively. Thus, as a general rule, those plumes plotting along the solid line delimiting coastal current existence are subject to stronger bottom trapping and horizontal compression than those plotting below that line, including our Patos and Plata plume realizations.

In Table 4, results based on our field data are bolded, and parameter values of other plumes given by Avicola and Huq (2002) are reproduced for comparison. Their tabulated results for the Plata plume (denoted A&H) are different from ours apparently because they used source parameters (inlet depth and density) appropriate to the head, rather than the mouth of the estuary. We excluded the estuary zone because its dynamics are ageostrophic, and thus inconsistent with their scheme's basic assumption that the plume is semi-geostrophic. However, for comparison, we include a calculation for the Patos plume using our data, but their assumed source characteristics (also denoted A&H).

The table rows and plot legend are sorted into a range of R/y_b values spanned by the Gaspe and the Rhine River plumes. On this scale, the Plata and Patos have only moderate isopycnal tilt. The Gaspe and Rhine plumes also span the h/H range, with the exception of the Patos, which is more extremely surface-advected than the Gaspe, unless the source conditions are those of the estuary head, in which case it resembles the Columbia or the Hudson. Both the Plata and Patos plumes thus classify as horizontally compressed at the base (with steep isopycnal slopes). The Patos is classified as surface-advected, while the Plata, being more inclined to bottom-trapping, classifies as intermediate. It is broader at its base than the Patos plume and has weaker geostrophic currents. The latter comparison is questionable, however: To the extent the Patos is ageostrophic (see Table 3), it may fail a key assumption of the A&H scheme. The Plata plume is also dimensionally deeper and broader than the Patos plume. This contrast holds whether the estuary head or mouth source parameters are used for the analysis. In terms of the non-dimensional parameters, the Plata closely resembles the Hudson plume dynamically, although in dimensional terms, it is actually deeper and broader, while the Patos resembles the Columbia plume, but is actually shallower and narrower. Depending upon source assumptions, the non-dimensional parameters imply that the Patos plume surface layer is only 1–2 m thick and feels the

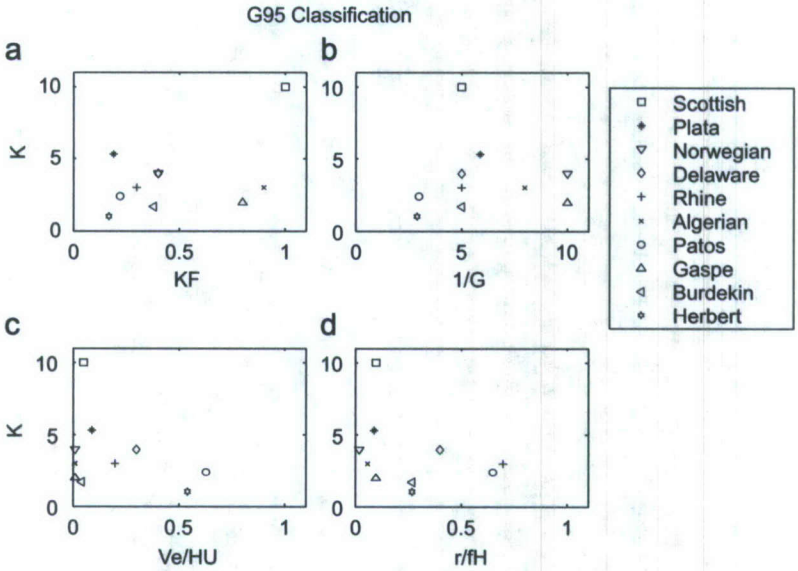

Fig. 7. The dynamical characteristics of various river plumes are shown using the Kelvin number, K, the primary parameter of the Garvine (1995) plume classification scheme. For each plume K, a non-dimensional horizontal plume scale, is plotted against the various secondary parameters representing (a) Coriolis effect, (b) aspect ratio, (c) Ekman transport and (d) basal friction.

Table 3
Momentum balance (non-dimensional) based on G95 parameters from their Table 4

Plume	Advective accel.	Coriolis accel.	Pressure gradient	Wind stress	Bottom stress
Along-shelf					
Patos	0.01	0.22	1	0.69	0.43
Plata	0	0.19	1	0.09	0.11
Across-shelf					
Patos	0	0.22	1	0.23	0.05
Plata	0	0.19	1	0.02	0

Pressure gradient is of order one, by definition.

Table 4
Non-dimensional parameters (cols. 2-3) derived from dimensional parameters (cols. 4-7) using A&H classification scheme (given to at least 2 significant figures)

Plume	h/H	R/y_b	h (m)	H (m)	R (km)	y_b (km)
Gaspe	0.12	8.6	12.9	111	9.3	1.1
Columbia	0.21	4.7	6.3	30	8.2	1.8
Patos (A&H)	**0.25**	**4.1**	**1.2**	**4.8**	**6.8**	**1.7**
Patos	**0.09**	**3.8**	**1.6**	**18**	**5.6**	**1.5**
Tsugaru	0.26	3.8	80.4	304	16	4.3
Plata A&H	0.41	2.4	3.9	9	13.4	5.5
Hudson	0.25	1.9	4.7	19	6.8	3.6
Plata	**0.25**	**1.8**	**6.6**	**27**	**10.8**	**6**
Chesapeake	0.59	0.7	9.7	17	6.5	9.7
Soya	1.8	0.6	69	39	14.1	24.7
Delaware	0.6	0.51	8.7	14	6.4	12.4
Rhine	0.92	0.15	10.6	12	5.5	37.2

Selected results reproduced from Avicola and Huq (2002) and their Table 1 and Fig. 11, which span the values of the Patos and Plata plumes, are included for comparison. Entries are sorted by decreasing R/y_b value.

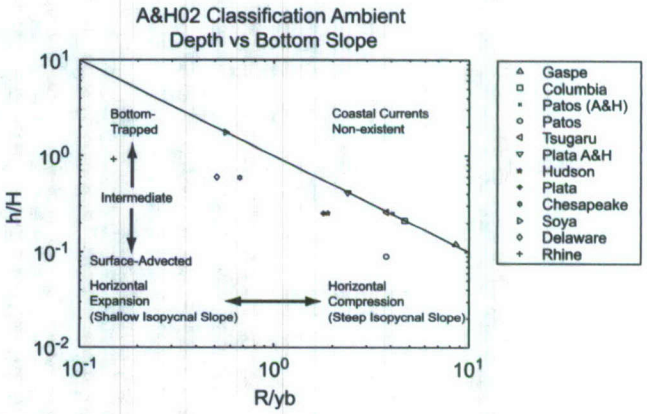

Fig. 8. The dynamical characteristics of various river plumes are shown by plotting the ambient depth parameter versus the bottom slope parameter of the Avicola and Huq (2002) plume classification scheme, using a log–log scale. The solid line indicates a dynamical limit above which coastal currents may not exist.

bottom only within 1–2 km of the shore and typically lies in water 5–20 m deep. In comparison, the Plata plume surface layer is 4–7 m deep, feels the bottom at most 5–6 km from shore and typically lies in water 10–30 m deep. These results are only partially supported by the shipboard CTD observations (Fig. 5a, c and e), which indicate a stronger tendency toward bottom trapping in both the Patos and Plata plumes. Plata plume isopycnal slopes indicate bottom trapping out to about 20 km offshore from Albardão and Rio Grande, but detachment from the bottom off Solidão. The Patos plume is not well resolved, but it appears to be bottom trapped close to the entrance. This observation is consistent with Avicola and Huq's Patos plume source scaling, but not with ours.

Under the circumstances in which we observed it, the Patos plume might be difficult to classify accurately. Firstly, it was only observed while already embedded in the Plata plume; the latter might have modified its characteristics in comparison with a corresponding isolated state. Secondly, the plume could have been producing a recirculation bulge, although this is less likely if the inflow is anticyclonic, frictional forces are active, or there was significant equatorward along-shelf flow, either buoyancy or wind driven (Nof and Pichevin, 2001; Fong and Geyer, 2002). The estimated inlet Rossby number, $Ro = ur/fLr$ (Fong and Geyer, 2002, see their Fig. 8 for corresponding model runs) is 0.54 and 0.00054 for the Patos and Plata plume, respectively. This implies a bulge on the Plata would be quite 'flat' with the bulk of the freshwater discharge going into the coastal current (75% for their model). For Patos, the bulge would be semi-circular, with about half going into the coastal current (45% in the model).

Given that the Patos plume along-shelf development was quite limited, the presence of a recirculation gyre would make it difficult to scale the resulting coastal current. The Patos plume shape suggests the presence of a recirculation gyre, with a large offshore bulge and short, but relatively narrow, equatorward coastal current. If the pattern of plume development is observed, the theory of Avicola and Huq (2003) can be used to predict the presence of such a gyre. If we use the observed plume width, at its maximum offshore extent (33 km) as an indicator of maximum separation distance, d, and compute the inertial turning radius, u/f, where f is the Coriolis parameter and u is the inlet velocity, we can calculate their separation parameter, df/u. Calculating u from the volume discharge rate and entrance geometry, we obtain a parameter value of about 30, which greatly exceeds their criterion (0.5) for recirculation gyre formation. However, this value must be regarded as uncertain because we are using climatological, rather than actual discharge ($2000\,m^3\,s^{-1}$), and it is likely an overestimate because we did not observe the plume at the time of its initial formation (and impact at the coast). If indeed a gyre has been formed, by the time of the survey it may well have grown considerably in extent, which would inflate the d estimate. On the other hand, if a gyre had not formed, a large bulge would not be evident and the plume width outside the entrance would not exceed, or at most would only slightly exceed, the coastal current width. Given this separation parameter estimate and observed plume shape, with a hook-shaped appearance indicating anticyclonic rotation, it seems likely that a recirculation gyre was present at the time of the survey.

The theory of Avicola and Huq (2002) avoids the issue of a bulge by assuming the plume discharge is parallel to the coast, which is not the case for the Patos, particularly since its training walls direct the plume immediately offshore, and even slightly upcoast (i.e. to the south, in the opposite direction to Kelvin wave propagation). We can, at least partially, account for the training wall effect by employing the inlet Kelvin number, K_i, following Garvine (1999), which scales the actual inlet width (0.75 km) by the internal Rossby radius. For the Plata and Patos plume, defining the inlet width at the mouth of the estuary, K_i is estimated to be, respectively, 0.05 and 13.5. These are extreme values indicating, respectively, a plume that is greatly expanded along-shelf (Plata) versus one that has very limited along-shelf penetration (Patos). The latter implies the Patos will have a surface anomaly map ($K_i \sim 0.1$, Garvine, 1999 and his Fig. 8) resembling that of a plume located very close to the equator, although the reason for this with the Patos plume, is the small inlet width, rather than a low value for the Coriolis parameter ($f = -7.7 \times 10^{-5}\,s^{-1}$, at Lat. 32°S). In either case, this implies very limited rotation influence, and is consistent with a plume that is almost symmetric with limited along-shore extent. This picture appears consistent with the Patos plume salinity field, as observed by STARRS (Fig. 3).

The model results given by Soares (2003) suggest that with a small K_i value the Patos estuarine outflow will be little affected by the Coriolis force, and will, instead, tend to be deflected by the coastal current. However, on a larger time scale, the river water will tend to mix with the seawater forming a large body of low salinity water that will obey the rotational dynamics of larger plumes. Soares (2003) considers that during the high discharge season, the plume resembles the supercritical diffusive type described by Chao (1988); it becomes supercritical during strong and short period high discharge events ($>4000\,m^3\,s^{-1}$) typical of the winter/spring season and ENSO events. The plume is not formed for typical summer river discharge values, which are lower than $700\,m^3\,s^{-1}$. Indeed, the Patos plume was absent during our subsequent summer (February, 2004) STARRS survey (results not shown). Instead, it was replaced by an 'inverted plume' with no freshwater outflow, but higher salinity shelf water penetrating the Lagoon.

The G99 scheme, which is based on a large number of numerical hydrodynamic model predictions, was less successful in predicting the observed along- and across-shelf penetration of the plumes (Patos and Plata penetrations were significantly over and underestimated, respectively), for reasons as yet undetermined, so those results are omitted here. This might have been due, at least in part, to significant wind stress influence, which is not incorporated into the G99 scheme.

Whitney and Garvine (2005) explicitly account for wind effects, using their wind strength index, W_S, a measure of the extent to which a plume's along-shelf flow is predominantly wind ($W_S > 1$) or buoyancy driven ($W_S < 1$). Our estimated value of W_S for the Patos and Plata plume is 1.9 indicating that wind influence dominates the effect of discharge on plume velocity. The significance of wind influence can also be gauged by employing the wind tilt time scale t_{tilt} of W&G, which is a measure of how long winds must persist to cause a significant change in the isopycnal tilt of the plume. t_{tilt} is estimated to be about 1 h and 2.5 day for the Patos and Plata plume, respectively. Thus, the Patos plume will respond almost immediately to wind changes, while the Plata will respond on time scales longer than one inertial period, i.e. within the weather band.

5. Discussion

Our observations and the resulting plume classification have a number of interesting implications, and coupled with our knowledge of the plume climatology, they raise several questions to guide further research.

During its winter and springtime extension in the equatorward direction, the Plata river typically penetrates beyond the entrance to the Patos Lagoon, while the Patos plume is relatively strong, at least in Spring. This, together with the greater geographic extent of the Plata plume and the discrepancy between their relative mean discharges ($25{,}000\,m^3\,s^{-1}$ for the Plata compared to $2000\,m^3\,s^{-1}$ for Patos), means that the winter and probably also the springtime Plata plume will likely fully embed, or otherwise merge with or overwhelm, the Patos plume.

Our observations show that, at least in the 2003 winter, the Patos plume maintained its integrity as a relatively symmetric, frictionally dominated plume with significant across-shelf, and modest along-shelf, development. The Plata plume on the other hand was highly asymmetric. Its along-shelf development was almost entirely confined to the equatorial side of its source region (the Río de la Plata) and it behaved dynamically like a buoyant coastal boundary current, with an approximately geostrophic across-shelf momentum balance. Both plumes were surface advected, but the Plata plume was deeper and broader.

This embedding of a small-scale plume (both in the sense of smaller physical size, and little rotation influence) within a larger-scale (physically larger, and rotationally dominated) plume has several implications.

Firstly, the embedded plume will be subject to advection by the larger plume and its dynamics will likely respond (at least to first order) as a small-scale plume debouching into an ambient long-shore current. This means, for example, that if the embedded plume tends to balloon to seaward (as the Patos appears to do, especially under high El Nino discharge conditions), forming a recirculation bulge (Nof and Pichevin, 2001; Fong and Geyer, 2002), the embedding (Plata) plume's coastal current will moderate this effect, by enhancing the downstream embedded (Patos) plume's coastal current, and decreasing its bulge growth rate. Secondly, the embedded plume will be subject to geostrophic current shear due to the tilt of the ambient plume isopycnal slopes (thermal wind). This will tend to enhance the equatorward coastal current nearer the surface and coast and (relatively speaking) diminish the flow (or reverse it) seaward and at depth, thus distorting the plume in the along-shelf direction by enhancing its (cyclonic) relative vorticity.

Both these effects would likely increase the aspect ratio of an embedded plume relative to one with otherwise similar parameters, which is not embedded. This suggests a need to modify the classification schemes that depend on this parameter (e.g., G95), to account for ambient shear.

Thirdly, being particularly susceptible to wind and bottom stress forcing, the Patos plume will be subject to advection and shear associated with changes in the effectiveness of wind and bottom stress as a function of water depth. Since the dynamics are essentially linear (the advective acceleration terms are negligible, see Table 2), any wind-driven advection and shear will add to the effects of the coastal current and background geostrophic shear associated with the ambient plume. The relative magnitude of the ambient buoyancy and wind-driven circulations will thus determine their relative influence on the embedded plume advection and shape.

6. Conclusions

Application of data from near-coincident airborne and in-situ surveys of the Plata and Patos plumes to dynamical classification schemes has elucidated the gross behavior and dynamics of the plumes, and has enabled likely implications of their mutual interaction to be identified. The Plata plume is dynamically of large scale, exhibiting a semi-geostrophic momentum balance, and responding primarily to seasonal, rather than weather-scale wind shifts. The Patos plume is only weakly affected by earth rotation, being dominated instead by weather-scale surface wind and bottom stress. In summer, the Patos plume is typically absent or only weakly developed, and the Plata plume is reduced in long-shelf extent, so that interaction between the plumes in this season is unlikely. In winter, prevailing downwelling favorable south-westerly winds cause the Plata plume to propagate northward, past the entrance to Patos Lagoon. The Patos plume, typically well developed in the spring, is found embedded in the hydrographic and current fields of the larger-scale Plata plume. The Plata plume will modify the environment of the embedded Patos plume by enhancing along-shelf advection and increasing ambient vertical and horizontal shear. Both these effects will tend to stretch and elongate the normally compact Patos plume in the along-shelf direction, but the likely intensity of this effect is yet to be determined. We hope to resolve this by comparing hydrodynamic model simulations of the Patos plume that are run both with and without an ambient Plata plume.

While the classification schemes account only for steady state forcing, studying various levels of forcing intensity can provide some insight into the likely transient response. An analysis of the momentum balance of the plumes shows that the advective acceleration terms are weak for the Patos and negligible for the Plata plume, suggesting that the dynamics are linear. Thus, to first order, the effects of independent forcings are additive. However, shear enhancement due to the ambient Plata plume could cause weak non-linear behavior in the Patos plume.

Without suitable current meter data, effects of transients could not be investigated empirically (e.g., by scaling the local acceleration), so the impact of rapid wind shifts and other forcing transients are unknown. However, the tilt time scale computed using the W&G scheme indicates that the shallow, frictionally dominated, Patos plume is likely to respond rapidly, on a time scale of about 1 h, to such transients. The deeper and larger Plata plume, being semi-geostrophic, will respond relatively slowly to wind transients. It will accelerate its along-shelf flow and adjust its across-shelf sea level gradient and isopycnal tilt, on time-scales of 2–3 days, to maintain geostrophic balance in the across-shelf direction. This would tend to enhance the ambient shear of an embedded Patos plume.

Our observations essentially comprise a snapshot of the Patos plume embedded within the wintertime Plata plume structure. The process by which the plumes actually merge and ultimately separate as the Plata plume expands in winter, engulfs the Patos plume and ultimately retracts in summer has not been observed. Numerical hydrodynamic model tests are presently being conducted to study the transient behavior of the plumes. These tests, which use realistic transient wind forcing are capable of simulating the merger and separation process. It is anticipated that they will yield significant useful insights into the mechanisms and dynamics of these processes. The implications for mixing between the two plume water masses and their ultimate fate as they are incorporated into the larger-scale deep ocean circulation are subjects for future investigation.

Acknowledgments

The Uruguayan Air Force (Brigada de Mantenimiento, Servicio de Sensores Remotos y Aeroespaciales, and Escuadrón de Transporte No. 3), provided aircraft, crew and logistics, and adapted the aircraft to STARRS. CITMPSA provided additional equipment and Aluminios del Uruguay donated mounting materials. Funding was provided by the Inter-American Institute for Global Change Research (IAI—Grant CRN-061), which is supported by the US National Science Foundation (Grant GEO-0452325), the Office of Naval Research Global (ONRG) and various academic and private institutions of Argentina, Brazil and Uruguay. Project leadership and coordination by Edmo Campos (University of Sao Paulo, Brazil) and Jerry Miller (formerly of NRL) are gratefully acknowledged. This paper is dedicated to the memory of Professor Richard W. Garvine, University of Delaware, and gratefully acknowledges his many enlightening contributions to the field of coastal ocean dynamics.

References

Avicola, G., Huq, P., 2002. Scaling analysis for the interaction between a buoyant coastal current and the continental shelf: experiments and observations. Journal of Physical Oceanography 32, 3233–3248.

Avicola, G., Huq, P., 2003. The role of outflow geometry in the formation of the recirculating bulge region in coastal buoyant outflows. Journal of Marine Research 61, 411–434.

Berdeal, I.G., Hickey, B.M., Kawase, M., 2002. Influence of wind stress and ambient flow on a high-discharge river plume. Journal of Geophysical Research 107 (C9), 13.1–13.24.

Burrage, D.M., Heron, M.L., Goodberlet, M., 2002a. Simulating passive microwave radiometer designs using SIMULINK. Simulation 78 (1), 36–55.

Burrage, D.M., Heron, M.L., Hacker, J.M., Stieglitz, T.C., Steinberg, C.R., Prytz, A., 2002b. Evolution and dynamics of tropical river plumes in the Great Barrier Reef: an integrated remote sensing and in situ study. Journal of Geophysical Research, Special Section on Salinity 107 (C12), SRF 17-1–SRF 17-22.

Burrage, D., Miller, J., Johnson, D., Wesson, J., Johnson, J., 2002c. Observing sea surface salinity in coastal domains using an Airborne Surface Salinity Mapper. In: Proceedings IEEE/MTS Marine Frontiers Oceans 2002, Biloxi, 29–31 October 2002 (Proceedings CDROM).

Burrage, D.M., Heron, M.L., Hacker, J.M., Miller, J.L., Stieglitz, T.C., Steinberg, C.R., Prytz, A., 2003. Structure and influence of tropical river plumes in the Great Barrier Reef: application and performance of an airborne sea surface salinity mapping system. Remote Sensing of the Environment 85 (2), 204–220.

Burrage, D.M., Wesson, J.C., Goodberlet, M.A., Miller, J.L., 2006. Optimizing performance of a microwave salinity mapper: STARRS L-band radiometer enhancements. Journal of Atmospheric and Oceanic Technology 25 (5), 776–793.

Burrage, D.M., Wesson, J.C., Martin, P.J., Martínez, C., Moller, Jr., O.O., Piola, A.R., 2008. Patos Lagoon outflow within the Rio de la Plata plume using an airborne salinity mapper: Modeling plume merger, in preparation.

Campos, E., Lorenzzetti, J., Stevenson, M., Stech, J.L., Souza, R., 1996. Penetration of waters from the Brazil–Malvinas Confluence region along the South American continental shelf up to 23°S. Anais Academia Brasileira de Ciências 68 (1), 49–58.

Chao, S.-Y., 1988. River-forced estuarine plumes. Journal of Physical Oceanography 18 (1), 72–88.

Fernandes, E.H.L., Dyer, K.R., Möller, O.O., Niencheski, L.F.H., 2002. The Patos Lagoon hydrodynamics during an El Nino event (1998). Continental Shelf Research 22, 1699–1713.

Fernandes, E.H.L., Marino-Tapia, I., Dyer, K.R., Möller, O.O., 2004. The attenuation of tidal and subtidal oscillations in the Patos Lagoon estuary. Ocean Dynamics 54 (3–4), 348–359.

Fong, D.A., Geyer, W.R., 2001. Response of a river plume during an upwelling favorable wind event. Journal of Geophysical Research 106 (C1), 1067–1084.

Fong, D.A., Geyer, W.R., 2002. The along-shore transport of freshwater in a surface-trapped river plume. Journal of Physical Oceanography 32, 957–972.

Framinan, M.B., Brown, O.T., 1996. Study of the Río de la Plata turbidity front, Part I: spatial and temporal distribution. Continental Shelf Research 16 (10), 1259–1282.

Garvine, R.W., 1995. A dynamical system for classifying buoyant coastal discharges. Continental Shelf Research 15 (13), 1585–1596.

Garvine, R.W., 1999. Penetration of buoyant coastal discharge onto the continental shelf: a numerical model experiment. Journal of Physical Oceanography 29, 1892–1909.

Guerrero, R.A., Acha, E.M., Framinan, M.B., Lasta, C.A., 1997. Physical oceanography of the Río de la Plata estuary, Argentina. Continental Shelf Research 17 (7), 727–742.

Hickey, B.M., Pietrfesa, L.J., Jay, D.A., Boicourt, W.C., 1998. The Columbia River plume study: subtidal variability in the velocity and salinity fields. Journal of Geophysical Research 103, 10,339–10,368.

Hubold, G., 1980a. Hydrography and plankton off southern Brazil and Río de la Plata, August–November 1977. Atlantica 4, 1–22.

Hubold, G., 1980b. Second report on hydrography and plankton off southern Brazil and Río de la Plata, autumn cruise: April–June 1978. Atlantica 4, 23–42.

Kourafalou, V.H., Oey, L.-Y., Wang, J.D., Lee, T.N., 1996a. The fate of river discharge on the continental shelf 1. Modeling the river plume and the inner shelf coastal current. Journal of Geophysical Research 101 (C2), 3415–3434.

Kourafalou, V.H., Lee, T.N., Oey, L.-Y., Wang, J.D., 1996b. The fate of river discharge on the continental shelf 2. Transport of coastal low-salinity waters under realistic wind and tidal forcing. Journal of Geophysical Research 101 (C2), 3435–3455.

Martinez, C.M., 2003. *The Plata winter cruise 2003*, Mar del Plata-Itajai 20 August–3 September 2003. Airborne Survey Summary Report, 6pp.

Masse, A.K., Murthy, C.R., 1992. Analysis of the Niagara River Plume dynamics. Journal of Geophysical Research 97 (C2), 2403–2420.

Miller, J.L., Goodberlet, M., 2004. Development and application of STARRS—a next generation airborne salinity imager. International Journal of Remote Sensing 25 (7–8), 1319–1324.

Möller, O.O., Castaing, P., 1999. Hydrological characteristics of the estuarine area of Patos Lagoon (30'S, Brazil). In: Perillo, G.M.E., Piccolo, M.C. (Eds.), Estuaries of South America (their Geomorphology and Dynamics)—Environmental Science. Springer, Berlin, pp. 83–100.

Möller Jr., O.O., Piola, A.R., 2004. The Plata summer cruise 2004, Cruise Report, 27 February 2004, 20pp.

Möller Jr., O.O., Castaing, P., Salomon, J.-C., Lazure, P., 2001. The influence of local and non-local forcing effects on the subtidal circulation of Patos Lagoon. Estuaries 24 (n2), 297–311.

Möller Jr., O.O., Lorenzzentti, J.A., Stech, J.L., Mata, M.M., 1996. The Patos Lagoon summertime circulation and dynamics. Continental Shelf Research 16, 335–351.

Möller Jr., O.O., Piola, A.R., Freitas, A.C., Campos, E.J.D., 2008. The effects of river discharge and seasonal winds on the Shelf off Southeastern South America. Continental Shelf Research, this issue, doi:10.1016/j.csr.2008.03.012.

Munchow, A., Garvine, R.W., 1993. Dynamical properties of a bouyancy-driven coastal current. Journal of Geophysical Research 98, 20063–20077.

Nof, D., Pichevin, T., 2001. The ballooning of outflows. Journal of Physical Oceanography 31, 3045–3058.

Pérez, T., Wesson, J., Burrage, D., 2006. Airborne remote sensing of the Río de la Plata plume using a microwave radiometer system. Sea Technology 47 (9), 31–34.

Piola, A.R., Campos, E.J.D., Möller, O.O., Charo, M., Martinez, C., 2000. Subtropical shelf front off eastern South America. Journal of Geophysical Research 105 (C3), 6566–6578.

Piola, A.R., Matano, R.P., Palma, E.D., Möller Jr., O.O., Campos, E.J.D., 2005. The influence of the Plata River discharge on the western South Atlantic shelf. Geophysical Research Letters 32, L01603.

Piola, A.R., Möller Jr., O.O., Guerrero, R.A., Campos, E.J.D., 2008. Variability of the Subtropical Shelf front off eastern South America: winter 2003 and summer 2004. Continental Shelf Research, this issue, doi:10.1016/j.csr.2008.03.013.

Piola, A.R., Möller Jr., O.O., Muelbert, J.H., 2003. *The Plata winter cruise 2003*. Cruise Report, 10 October 2003, 20pp.

Pullen, J.D., Allen, J.S., 2000. Modeling studies of the coastal circulation off Northern California: shelf response to a major Eel river flood event. Continental Shelf Research 20, 2213–2238.

Prytz, A., Heron, M. L., Burrage, D., Goodberlet, M., 2002. Calibration of the scanning low frequency microwave radiometer. In: Proceedings IEEE/MTS Oceans 2002, 29–31 October, Biloxi, USA, 2002 (Proceedings CDROM).

Soares, I.D., 2003. The Southern Brazilian shelf buoyancy-driven currents. Ph.D. Thesis, RSMS, University of Miami, FL, USA, 317pp.

Soares, I., Möller Jr., O., 2001. Low-frequency currents and water mass spatial distribution on the southern Brazilian shelf. Continental Shelf Research 21, 1785–1814.

Souza, R.B., Robinson, I.S., 2004. Lagrangian and satellite observations of the Brazilian Coastal Current. Continental Shelf Research 24, 241–262.

Simionato, C.G., Nunez, M.N., 2001. The salinity front of the Río de la Plata—a numerical case study for winter and summer conditions. Geophysical Research Letters 28, 132641–132644.

Stumpf, R.P., Gelfenbaum, G., Pennock, J.R., 1993. Wind and tidal forcing of a buoyant plume, Mobile Bay, Alabama. Continental Shelf Research 13 (11), 1281–1301.

Vaz, A.C., Möller Jr., O.O., Almeida, T.L., 2006. Sobre a descarga dos rios afluentes à Lagoa dos Patos. Atlântica 28, 13–23.

Wells, P.G., Daborn, G.R. (Eds.), 1997. The Río de la Plata—An Environmental Overview. Dalhousie University, Halifax, Nova Scotia, p. 248.

Whitney, M.M., Garvine, R.W., 2005. Wind influence on a coastal buoyant outflow. Journal of Geophysical Research 110, C03041.

Xing, J., Davies, A.M., 1999. The effect of wind direction and mixing upon the spreading of a buoyant plume in a non-tidal regime. Continental Shelf Research 19, 1437–1483.

Yankovsky, A.E., 2000. The cyclonic turning and propagation of buoyant coastal discharge along the shelf. Journal of Marine Research 58 (4), 585–607.

Yankovsky, A.E., Chapman, D.C., 1997. A simple theory for the fate of buoyant coastal discharges. Journal of Physical Oceanography 27 (7), 1386–1401.

Zavialov, P.O., Möller, O.O., 2000. Ship/helicopter survey of Patos-Mirim Lagoon Plume. In: Proceedings of the 32nd International Liege Colloquium on Ocean Hydrodynamics, Exchange Processes at the Ocean Margins, Liege, 8–12 May 2000, 79pp.

Zavialov, P.O., Kostianoy, A.G., Möller Jr., O.O., 2003. SAFARI cruise: mapping river discharge effects on Southern Brazilian shelf. Geophysical Research Letters 30 (21), 2126 OCE7-1-4.

Zavialov, P., Möller, O., Campos, E., 2002. First direct measurements of currents on the continental shelf of Southern Brazil. Continental Shelf Research 22, 1975–1986.